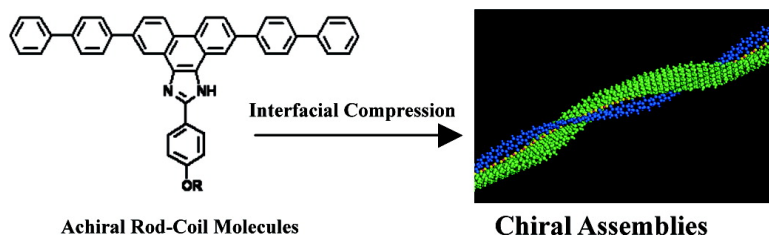


## Chiral Assembly from Achiral Rod-Coil Molecules Triggered by Compression at the Air#Water Interface

Libin Liu, Dong-Je Hong, and Myongsoo Lee

*Langmuir*, 2009, 25 (9), 5061-5067 • DOI: 10.1021/la804043z • Publication Date (Web): 20 March 2009

Downloaded from <http://pubs.acs.org> on May 1, 2009



### More About This Article

Additional resources and features associated with this article are available within the HTML version:

- Supporting Information
- Access to high resolution figures
- Links to articles and content related to this article
- Copyright permission to reproduce figures and/or text from this article

[View the Full Text HTML](#)

Chiral Assembly from Achiral Rod–Coil Molecules Triggered by  
Compression at the Air–Water Interface

Libin Liu, Dong-Je Hong, and Myongsoo Lee\*

Center for Supramolecular Nano-Assembly, Department of Chemistry, Yonsei University, Seoul 120-749, Korea

Received December 8, 2008. Revised Manuscript Received February 19, 2009

A series of achiral rod–coil molecules consisting of an oligo(*p*-phenylene) conjugated rod with a poly(ethylene oxide) or poly(propylene oxide) coil laterally attached through an imidazole linkage were synthesized, and their interfacial behaviors were investigated. Compounds **1a** and **1b** have a similar surface behavior with a shoulder indicating a transformation of rod segments from flat-on to vertical orientation. Interestingly, CD and AFM suggest chiral films are formed when the LB films were deposited after the shoulder. Although compound **1c** shows different surface behavior because the PEO chains dissolved into water upon compression, macroscopic chirality was also detected. In contrast, compound **2**, based on a reduced conformational rigidity of the aromatic rod segment, does not form chiral assemblies. Combining the data collected, the cooperative interaction of the hydrogen bond between the molecules and  $\pi$ – $\pi$  stacking as well as the steric constraint between the aromatic rod segments are responsible for the macroscopic chirality. Such kind of stacking can be realized through a molecular design and a lateral compression. A deep insight into the relationship between the molecular structure and the chirality was gained.

## Introduction

Chirality is a basic character of nature and appears at various hierarchical levels from molecular to supramolecular levels.<sup>1</sup> While the origin of homochirality in nature is still unresolved, great efforts have been devoted to the design and application of chiral molecules and supramolecular systems in recent years. This includes enantioselective catalysts, chiral separation/resolution, immobilization of bioactive materials through chiral molecular recognition, chiral sensors, and chiroptical switches.<sup>2,3</sup> Most of the previously reported chiralities are based on chiral building blocks or chiral template.<sup>2–5</sup> However, optically active

supramolecular assemblies can also be realized on the exclusive basis of achiral molecules.<sup>6–10</sup> For instance, some achiral dyes and achiral inorganic salts have been reported to form optically active supramolecular assemblies and crystals, respectively, under circularly polarized light irradiation or a directional stirring.<sup>8,9</sup> Aida and co-workers have demonstrated that spin-coating of hydrogen-bonded achiral dendritic zinc porphyrin J-aggregates gives optically active films.<sup>10</sup> The chiral supramolecular assemblies achieved by achiral molecules are attracting great interest as useful models for the spontaneous mirror-symmetry breaking in nature and for the formation of polymers of homochiral sequences from mixtures of racemic monomers.

Interfacial assembly through the Langmuir as well as the Langmuir–Blodgett (LB) technique offers excellent arenas for constructing supramolecular assemblies or ultrathin organized molecular films of the functional materials.<sup>11</sup> By taking advantage of this technique, not only the molecular orientation but also the molecular arrangement as well as the aggregation can be modulated to some extent in a two-dimensional manner.<sup>11,12</sup> Organic  $\pi$ -conjugated systems are attractive materials to be used as active components in optoelectronic device ranging in size from molecular to macroscopic dimensions. Rod–coil molecules as a typical  $\pi$ -conjugated system consisting of conformationally rigid rod and flexible coil blocks in a molecular structure have been widely investigated in solution and in solid states,<sup>13,14</sup> while the investigations concerning thin-film structures of rod–coil molecules by

\*To whom correspondence should be addressed. E-mail: mslee@yonsei.ac.kr.

(1) Special issue on supramolecular chirality: *Top. Curr. Chem.* **2006**, *265*, 1.

(2) (a) Feringa, B. L.; van Delden, R. A. *Angew. Chem., Int. Ed.* **1999**, *38*, 3418–3438. (b) Feringa, B. L. *Acc. Chem. Res.* **2001**, *34*, 504–513. (c) Feringa, B. L.; van Delden, R. A.; Koumura, N.; Geertsema, E. M. *Chem. Rev.* **2000**, *100*, 1789–1816. (d) Pijper, D.; Jongejan, M. G. M.; Meetsma, A.; Feringa, B. L. *J. Am. Chem. Soc.* **2008**, *130*, 4541–4552.

(3) (a) Pu, L. *Chem. Rev.* **2004**, *104*, 1687–1716. (b) Hazen, R. M.; Sholl, D. S. *Nat. Mater.* **2003**, *2*, 367–374. (c) Sato, O. *Acc. Chem. Res.* **2003**, *36*, 692–700.

(4) (a) Rowan, A. E.; Nolte, R. J. M. *Angew. Chem., Int. Ed.* **1998**, *37*, 63–68. (b) Hirschberg, J. H. K. K.; Brunsveld, L.; Ramzi, A.; Vekemans, J. A. J. M.; Sijbesma, R. P.; Meijer, E. W. *Nature (London)* **2000**, *407*, 167–170.

(5) For recent reviews, see: (a) Würthner, F. *Chem. Commun.* **2004**, 1564–1579. (b) Shimizu, T.; Masuda, M.; Minamikawa, H. *Chem. Rev.* **2005**, *105*, 1401–1443. (c) Hoebein, F. J. M.; Jonkheijm, P.; Meijer, E. W.; Schenning, A. P. H. *J. Chem. Rev.* **2005**, *105*, 1491–1546. (d) Wu, J.; Pisula, W.; Müllen, K. *Chem. Rev.* **2007**, *107*, 718–747.

(6) (a) Prins, L. J.; Huskens, J.; de Jong, F.; Timmerman, P.; Reinhoudt, D. N. *Nature (London)* **1999**, *398*, 498–502. (b) Yashima, E.; Maeda, K.; Okamoto, Y. *Nature (London)* **1999**, *399*, 449–451. (c) Yang, W. S.; Chai, X. D.; Chi, L. F.; Liu, X. D.; Cao, Y. W.; Lu, R.; Jiang, Y. S.; Tang, X. Y.; Fuchs, H.; Li, T. J. *Chem.—Eur. J.* **1999**, *5*, 1144–1149.

(7) (a) Saito, Y.; Hyuga, H. *J. Phys. Soc. Jpn.* **2005**, *74*, 535–537. (b) Kondepudi, D. K.; Asakura, K. *Acc. Chem. Res.* **2001**, *34*, 946–954. (c) Kondepudi, D. K.; Bullock, K. L.; Digits, J. A.; Hall, J. K.; Miller, J. M. *J. Am. Chem. Soc.* **1993**, *115*, 10211–10216. (d) Ezuhara, T.; Endo, K.; Aoyama, Y. *J. Am. Chem. Soc.* **1999**, *121*, 3279–3283.

(8) (a) Ribó, J. M.; Crusats, J.; Sagués, F.; Claret, J.; Rubires, R. *Science* **2001**, *292*, 2063–2066. (b) Rubires, R.; Farrera, J.-A.; Ribó, J. M. *Chem.—Eur. J.* **2001**, *7*, 436–446.

(9) (a) Link, D. R.; Natale, G.; Shao, R.; MacLennan, J. E.; Clark, N. A.; Kórblova, E.; Walba, D. M. *Science* **1997**, *278*, 1924–1927. (b) Pawlik, A.; Kirstein, S.; De Rossi, U.; Daehne, S. *J. Phys. Chem. B* **1997**, *101*, 5646–5651. (c) De Rossi, U.; Dähne, S.; Meskers, S. C. J.; Dekkers, H. P. J. M. *Angew. Chem., Int. Ed. Engl.* **1996**, *35*, 760–763.

(10) Yamaguchi, T.; Kimura, T.; Matsuda, H.; Aida, T. *Angew. Chem., Int. Ed.* **2004**, *43*, 6350–6355.

(11) Ulman, A. *An Introduction to Ultrathin Organic Films—From Langmuir–Blodgett to Self-Assembly*; Academic Press: Boston, 1991.

(12) Chen, X.; Lenthert, S.; Hirtz, M.; Lu, N.; Fuchs, H.; Chi, L. *Acc. Chem. Res.* **2007**, *40*, 393–401, and references therein.

(13) (a) Jenekhe, S. A.; Chen, X. L. *Science* **1999**, *283*, 372–375. (b) Klok, H.-A.; Lecommandoux, S. *Adv. Mater.* **2001**, *13*, 1217–1229.

(14) (a) Lee, M.; Cho, B.-K.; Zin, W.-C. *Chem. Rev.* **2001**, *101*, 3869–3892. (b) Ryu, J.-H.; Oh, N.-K.; Zin, W.-C.; Lee, M. *J. Am. Chem. Soc.* **2004**, *126*, 3551–3558. (c) Lee, M.; Park, M.-H.; Oh, N.-K.; Zin, W.-C.; Jung, H.-T.; Yoon, D.-K. *Angew. Chem., Int. Ed.* **2004**, *43*, 6465–6468. (d) Kim, J.-K.; Hong, M.-K.; Ahn, J.-H.; Lee, M. *Angew. Chem., Int. Ed.* **2005**, *44*, 328–332. (e) Kim, J.-K.; Lee, E.; Jeong, Y.-H.; Lee, J.-K.; Zin, W.-C.; Lee, M. *J. Am. Chem. Soc.* **2007**, *129*, 6082–6083.

the LB technique on a solid support are rarely found.<sup>15,16</sup> Moreover, there is no report on the fabrication of optically active molecular assemblies from achiral rod-coil molecules without introduction of external chiral factors. Herein, we have demonstrated that supramolecular chirality could be achieved by a series of rationally designed achiral rod-coil molecules. The cooperative interactions of the intermolecular hydrogen bond and  $\pi$ - $\pi$  stacking are responsible for the macroscopic chirality. Additionally, the steric constraint between the aromatic rod segments is crucial for the chiral assemblies formation.

### Experimental Section

**Materials.** The amphiphilic rod-coil molecules described here consist of an oligo(*p*-phenylene) conjugated rod with a poly(ethylene oxide) (PEO) or poly(propylene oxide) (PPO) coil laterally attached through an imidazole linkage. The synthetic procedures and characterization are described in the Supporting Information. The resulting rod-coil amphiphiles were characterized by <sup>1</sup>H and <sup>13</sup>C NMR spectroscopy, elemental analysis, and matrix-assisted laser desorption ionization time-of-flight (MALDI-TOF) mass spectroscopy and were shown to be in full agreement with the structures presented (Figure 1).

**Monolayer Fabrication.** Langmuir isotherms at the air-water interface and Langmuir-Blodgett (LB) depositions onto a solid substrate were conducted at room temperature using a KSV 2000 LB minitrough. A 40–120  $\mu$ L volume of dilute molecule solution (concentration less than 0.5 mg/mL) in chloroform (HPLC grade) was deposited in 5–10 drops uniformly distributed onto the water surface (Nanopure, 18.2 M $\Omega$  cm) and left to evaporate and spread evenly over a period of 30 min. The limiting cross-sectional area was determined at the steep rise in the surface pressure related to the formation of condensed monolayer. For AFM measurement, the monolayer LB films of the molecules were transferred at a rate of 2 mm/min onto silicon wafers at various surface pressures by the upstroke mode of the vertical dipping method. For UV-vis, CD, and FT-IR spectral measurements, the floating films were transferred onto quartz and ZnSe solid supports at selected surface pressure by the horizontal Langmuir-Schaefer method and by a certain number of depositions.

Highly polished [100] silicon wafers (Semiconductor Processing Co.) were cut into rectangular pieces (2  $\times$  2 cm<sup>2</sup>) and sonicated in Nanopure water for 10 min to remove silicon dust. The wafers were then chemically treated with “piranha solution” (30% concentrated hydrogen peroxide, 70% concentrated sulfuric acid, *hazardous solution!*) for 1 h and then washed with abundant Nanopure water.

**Monolayer Characterization.** The LB monolayers on the silicon substrates were studied with a Nanoscope IIIa Multi-mode AFM. Scans were performed in the “light” tapping mode in accordance with the usual procedure adapted in our laboratory.<sup>17</sup> An amplitude ratio of 0.95 and higher was employed to avoid monolayer damage.<sup>18</sup> The domain topography and the surface area coverage were calculated from height histograms using the bearing analysis.<sup>19</sup> AFM characterization of the deposited LB films was done after drying in a desiccator for

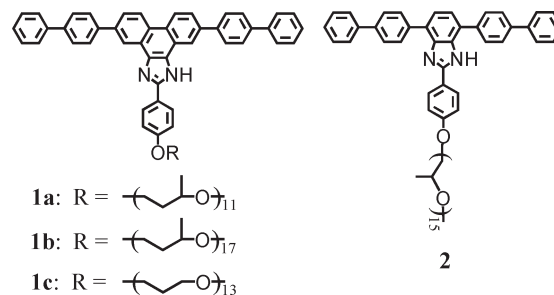


Figure 1. Molecular structures of 1a, 1b, 1c, and 2.

24 h. The AFM scans were conducted at 0.5–2 Hz scanning rate. The AFM tip radii were between 20 and 35 nm, and the spring constants of these cantilevers were in the range of 40–60 N/m. UV-vis and circular dichroism (CD) measurements of the films were performed at room temperature using a UV-1650PC and JASCO J-810CD spectrophotometer, respectively. In the measurement of the CD spectra, the multilayer films were placed perpendicular to the light path and rotated within the film plane in order to avoid the polarization-dependent reflections and eliminate the possible angle dependence of the CD signal.<sup>20</sup> FT-IR measurements were recorded on Equinox 55 FT-IR spectrophotometer with an average of several hundred scans.

### Results and Discussion

**Interfacial Behavior of 1a.** The surface pressure–area ( $\pi$ - $A$ ) isotherm of 1a reveals stable Langmuir monolayer at the air-water interface as shown in Figure 2a. A steadily rising surface pressure is recorded up to the surface pressure of 12 mN/m, and a shoulder appears. Constant compression leads to a sharp increase in the surface pressure and finally the monolayer collapses at 35 mN/m. Before and after the shoulder, the limiting cross-sectional molecular areas calculated by the extrapolation the steep rise in the surface pressure to a zero level are 4.55 and 3.04 nm<sup>2</sup>, respectively. The values, which are just before the shoulder on the large molecular area side and just before the film collapse, are consistent with the area occupied by a molecule in the flat-on and vertical orientation, which are about 4.47 and 3.11 nm<sup>2</sup>, respectively.<sup>21</sup> Therefore, the shoulder in the isotherm likely indicates a transformation of the aromatic rod segment of the molecule from flat-on to vertical orientation upon compression.

Reversibility of the monolayer behavior at the air-water interface was tested by repeating compression–expansion cycles several times for the monolayer at a surface pressure of 10 mN/m (Figure S1). A very modest hysteresis was observed for each cycle indicating modest creep and a short recovery time for the PPO chains to expand to the original random coil conformation. The stability of the spreading films on the water surface was also evaluated by measuring the  $\pi$ - $t$  or  $A$ - $t$  isotherms (Figure 2b). The monolayer was compressed to a

(15) (a) Li, H. B.; Liu, Q. T.; Xu, M.; Bu, W. F.; Lin, X. K.; Wu, L. X.; Shen, J. C. *J. Phys. Chem. B* **2005**, *109*, 2855–2861. (b) Zhang, J.; Cao, H. Q.; Wan, X. H.; Zhou, Q. F. *Langmuir* **2006**, *22*, 6587–9592.

(16) (a) Tsukruk, V. V.; Genson, K.; Peleshanko, S.; Markutsya, S.; Lee, M.; Yoo, Y.-S. *Langmuir* **2003**, *19*, 495–499. (b) Holzmüller, J.; Genson, K. L.; Park, Y.; Yoo, Y.-S.; Park, M.-H.; Lee, M.; Tsukruk, V. V. *Langmuir* **2005**, *21*, 6392–6398. (c) Liu, L.; Moon, K.-S.; Gunawidijaja, R.; Lee, E.; Tsukruk, V. V.; Lee, M. *Langmuir* **2008**, *24*, 3930–3936. (d) Liu, L.; Kim, J.-K.; Lee, M. *ChemPhysChem* **2008**, *9*, 1585–1592.

(17) Tsukruk, V. V.; Reneker, D. H. *Polymer* **1995**, *36*, 1791–1808.

(18) Magonov, S. N.; Elings, V.; Whangbo, M. H. *Surf. Sci.* **1997**, *375*, L385–L391.

(19) Magonov, S. N. *Surface Analysis with STM and AFM: Experiment and Theoretical Aspects of Image Analysis*; VCH: New York, 1996.

(20) Spitz, C.; Dähne, S.; Ouart, A.; Abraham, H.-W. *J. Phys. Chem. B* **2000**, *104*, 8664–8669.

(21) The surface area occupied by the aromatic rod segments was calculated by the Corey–Pauling–Koltun (CPK) mode to be about 2.27 nm<sup>2</sup> in the flat-on orientation ( $A_{\text{rod||}}$ ) and 0.91 nm<sup>2</sup> in the vertical orientation ( $A_{\text{rod}\perp}$ ). The surface area of PPO chains ( $A_{\text{PPO}}$ ) was estimated by the area occupied by ethylene oxide chains (the methyl group would be exposed to air). The surface area of the ethylene oxide monomeric units oriented at the water surface and hydrogen-bonded with 1–3 water molecules is about 0.22–0.28 nm<sup>2</sup> (Cox, J. K.; Yu, K.; Eisenberg, A.; Lennox, R. B. *Phys. Chem. Chem. Phys.* **1999**, *1*, 4417–4421. Fauré, M. C.; Bassereau, P.; Carignano, M. A.; Szleifer, I.; Gallot, Y.; Andelman, D. *Eur. Phys. J. B* **1998**, *3*, 365–375). Therefore, the surface area occupied by a molecule is calculated as  $A_{\text{rod||}} + A_{\text{PPO}}$  in the flat-on orientation or  $A_{\text{rod}\perp} + A_{\text{PPO}}$  in the vertical orientation.

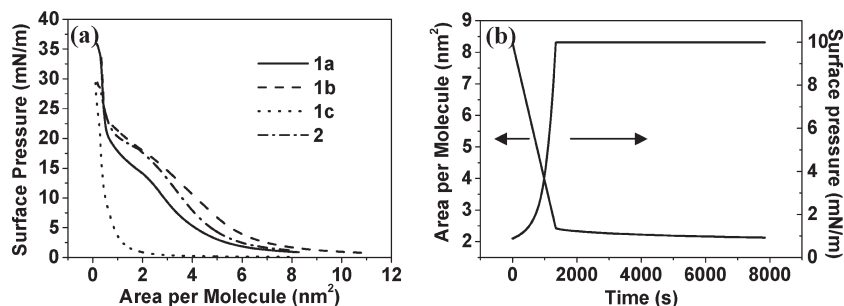


**Figure 2.** (a) Surface pressure–area isotherms of the rod–coil molecules at the air–water interface. (b) Changes of **1a** in the surface area as a function of time and at a constant surface pressure of 10 mN/m.

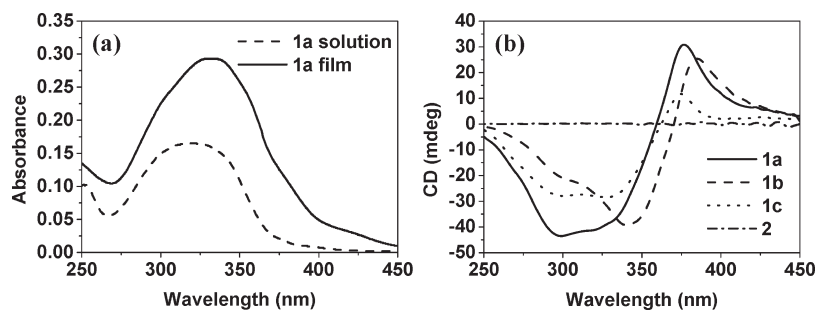


**Figure 3.** (a) UV–vis spectra of **1a** in  $\text{CHCl}_3$  solution and in LB films. (b) CD spectra of the LB films for different molecules.

surface pressure of 10 mN/m and held constant at this value for a period of 120 min. The area per molecule decreased about  $25 \text{ \AA}^2$  over the 120 min period. This value corresponds to  $< 8\%$  of the limiting molecular area of the monolayer. This slight decrease in the surface area is due to the rearrangement of the molecules to reduce the empty spaces in the monolayer or a partial aggregation of the molecules. Therefore, the film kinetic data suggest that a relative stable monolayer was formed at the air–water interface.

**Chiral Film of 1a.** The monolayer was transferred onto the solid substrate, and a typical transfer ratio was in the range of 0.8–0.9, which suggests a good film quality. The UV–vis spectra of a 25-layer LB film deposited after the shoulder (at 18 mN/m) exhibit a strong absorption at 333 nm and a shoulder at 300 nm. The two bands could be ascribed to  $\pi$ – $\pi^*$  transition and charge-transfer bands, respectively. The UV–vis spectra of **1a** dissolved in chloroform exhibit an inhomogeneously broadened  $\pi$ – $\pi^*$  absorption band centered at 318 nm. This absorption band shows no resolved vibrational fine structure and is associated with a conformationally disordered molecular chain (Figure 3a). The absorption peak of the  $\pi$ – $\pi^*$  transition of the LB films is red-shifted by 15 nm with respect to that of chloroform solution, indicating that a sort of head-to-tail arrangement of the molecules in the J-aggregates is formed in the LB films.<sup>22</sup>

It is interesting to note that when the films were subjected to circular dichroism (CD) measurements, a bisignate CD signal associated with a  $\pi$ – $\pi^*$  absorption band exhibiting a positive Cotton effect at high wavelength and a negative Cotton effect at low wavelength with a crossover at 358 nm was detected (Figure 3b). This CD couplet is character-

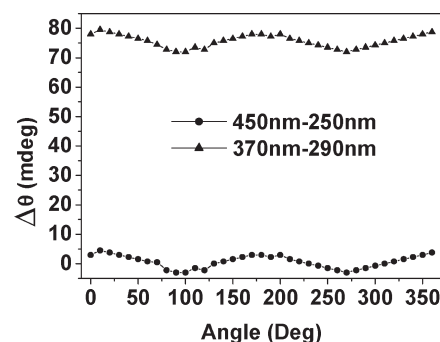


**Figure 4.** Angle dependence of the CD amplitude (triangles) and the background (dots) of the CD spectra when the LB film of **1a** was rotated in a step of  $10^\circ$  within the sample plane.

istic of exciton coupling between neighboring polymer chains in a helical orientation.<sup>23</sup> The peak at 298 nm in the CD spectra could be regarded as a charge-transfer band, which appeared in the shoulder at 300 nm of the UV–vis absorbance.

To solidly confirm that the supramolecular chirality in the LB film is really from the packing of **1a** molecule, not from parasitic artifacts which originate from the interaction between the macroscopic anisotropies such as birefringence and linear dichroism, we have measured the angle dependence of the CD spectra.<sup>20</sup> The sample was placed perpendicular to the light path to avoid birefringence contribution and rotated in a step of  $10^\circ$  around the optical axis. The angle dependence of the CD amplitude is determined by the difference between maximum value at 370 nm and minimum value at 290 nm, and the corresponding angle dependence of the background is determined by the difference between the values at upper wavelength edge at 450 nm and lower edge at 250 nm as shown in Figure 4. Both amplitudes can be approximated by a  $\cos(2\beta)$  function. The cosine function of the background situate around 0 mdeg, while that of the sample is positively shifted about 75 mdeg compared with that of

(22) (a) Kim, J.; Swager, T. M. *Nature (London)* **2001**, *411*, 1030–1034. (b) Kim, J.; Levitsky, I. A.; McQuade, D. T.; Swager, T. M. *J. Am. Chem. Soc.* **2002**, *124*, 7710–7718.

(23) (a) Langeveld-Voss, B. M. W.; Janssen, R. A. J.; Christiaans, M. P. T.; Meskers, S. C. J.; Dekkers, H. P. J. M.; Meijer, E. W. *J. Am. Chem. Soc.* **1996**, *118*, 4908–4909. (b) Langeveld-Voss, B. M. W.; Beljonne, D.; Shuai, Z.; Janssen, R. A. J.; Meskers, S. C. J.; Meijer, E. W.; Brédas, J. L. *Adv. Mater.* **1998**, *10*, 1343–1348.

the background. This is a clear indication that intrinsic chirality really exists in the LB film of **1a**.

Atomic force microscopy (AFM) experiments were performed on one-layer LB films to further confirm the structures. Transferred monolayer of **1a** onto a silicon substrate before the shoulder by vertical dipping method reveals smooth and uniform film (Figure 5a). Remarkably, AFM images of the LB films deposited after the shoulder (at 15 mN/m) show fibrillar structures (Figure 5b,c). The individual fibrils have an average height of 1.4 nm and average width of 13 nm (dimensions after correction for tip-broadening effect<sup>24</sup>). The structural dimensions of  $\sim 1:10$  ratio of height and width indicate that these structures are likely the wide ribbons. The height of the ribbons is close to the height of the rod segments adopting stand-up conformation to be about 1.3 nm calculated by CPK mode. The width of the ribbons is compatible with two molecular length of 11–15 nm with PPO chains surrounded along the backbone in an extended conformation. This is consistent with the result of the  $\pi$ -*A* isotherm that after the shoulder the aromatic rod segments of the molecules are suggested to have a vertical arrangement and the flexible chains are surrounded along the rod segments. Further compression leads to the ribbons becoming more densely packed and orienting in the dipping direction, indicating that the microscopic ordering is controlled by the capillary forces in the course of the LB deposition (Figure 5d).

We tried to find some kinds of pitch of these ribbons by AFM; unfortunately, it could not be clearly visualized. This may be due to that the PPO chains are surrounded along the rod-stacking backbone and space-filling of the flexible coil chains. We also performed AFM measurement of multilayers and CD spectra of the corresponding layers. In all cases, AFM images show the full area coverage of the Langmuir–Blodgett film and a high film-transfer ratio (0.8–0.9) of every layer. This indicates that the morphology of the formed films at the air–water interface is preserved upon transfer.<sup>25</sup> Similar ill-defined ribbons were observed for different multilayers (Figure S2). This is reasonable for AFM measurements because only the most outer layer of the LB films were scanned. The increase in the number of the layer will only lead to the increase in the thickness of the film. The CD spectra also revealed the consistent results (Figure S3). As the number of the layer increased, the intensity of the CD signal increased.

**Coil Effect on the Interfacial Behavior and Supramolecular Chirality.** To investigate the coil effect on the interface behavior and supramolecular chirality, rod–coil homologues with a longer PPO chain (**1b**, Figure 1) and a PEO chain (**1c**, Figure 1) instead of PPO chain were investigated. For **1b**, a similar shape of the  $\pi$ -*A* isotherm compared with that of **1a** was obtained (Figure 2a). Because of the longer PPO chain, **1b** occupies more molecular area at low surface pressure, and therefore the transition surface pressure appears at relatively higher surface pressure of 15 mN/m. Whereas for **1c**, a very different isotherm was obtained (Figure 2a). The shape of the isotherm is similar to our previously reported PEO-containing rod–coil molecule.<sup>16c</sup> The steep increase in the surface pressure at the molecular area below 1 nm<sup>2</sup> is due to the crowding of the aromatic rods upon compression after the PEO chains became completely submerged into the water subphase. Although there is no shoulder appeared in the isotherm, the limiting

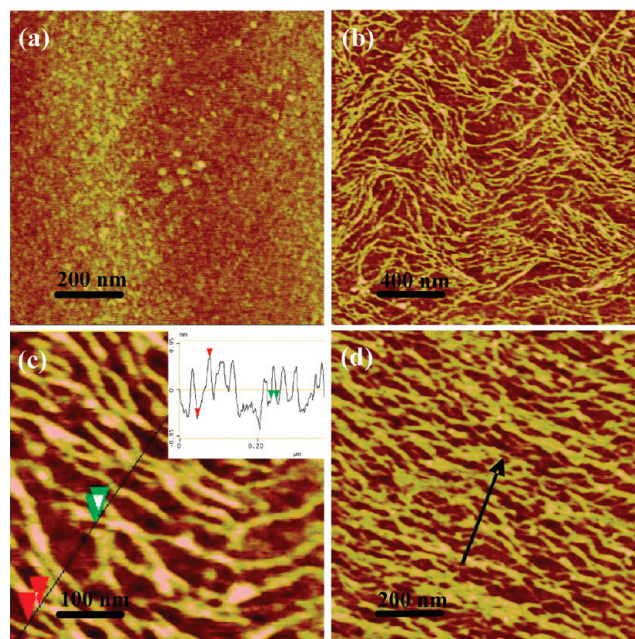


**Figure 5.** AFM images of one-layer LB films of **1a** deposited at different surface pressure: (a) at 5 mN/m; (b, c) at 15 mN/m. Inset is the height profile along the line. (d) At 18 mN/m. Arrow indicates the dipping direction.

cross-sectional area calculated by the extrapolation of the steep rise in the surface pressure to a zero level is 0.98 nm<sup>2</sup>, demonstrating that the rod segments adopt a vertical orientation in a compressed state,<sup>21</sup> similar to the results of **1a** and **1b**. The UV–vis spectra of 20-layer LB films deposited at the surface pressure of 20 mN/m for **1b** and **1c** are almost the same as that of **1a** (Figure S4). The red-shifted spectra of the LB film with respect to that of the chloroform solution indicate that the molecules are formed J-aggregates in the LB films. Notably, the CD spectra reveal the similar bisignate Cotton effect with a positive signal at high wavelength and a negative signal at low wavelength (Figure 3b, Figure S5). This indicates that the coil chain causes a different interface behavior, but supramolecular chirality still exists in the LB films. The crossover of the CD signal for the three molecules appears at different positions. This could be regarded as due to the inhomogeneous packing of the rod segments in the LB films.

AFM images of one-layer LB film of **1b** deposited at low surface pressure reveal featureless and uniform films (Figure 6a), while after the shoulder, at the surface pressure of 20 mN/m, similar ill-defined ribbons were obtained compared with that of **1a** (Figure 6b). Whereas for **1c**, the films deposited at different surface pressure reveal nanorod structures with an average height of 1.5 nm (Figure 6c–e). This value is also compatible with the height of aromatic rod segments in stand-up conformation atop on the PEO layers. When deposited onto a substrate, PEO chains adsorb onto the hydrophilic surface underneath the hydrophobic backbone, which translates into increased height of the nanorods. Although no distinct helical structure could be observed from AFM images, their CD spectra strongly suggest that the molecules are aligned in a helical sense conformation.

All the data made us draw the conclusion that the CD signal obtained in the LB films is due to the hydrogen bond formation between the imidazole units of the molecules. We suggest that the nitrogen in the imidazole of the rod–coil molecule could form H-bonds with the hydrogen in the N–H

(24) Samori, P.; Francke, V.; Mangel, T.; Mullen, K.; Rabe, J. P. *Opt. Mater.* **1998**, *9*, 390–393.

(25) (a) Genson, K. L.; Vaknin, D.; Villacencio, O.; McGrath, D. V.; Tsukruk, V. V. *J. Phys. Chem. B* **2002**, *106*, 11277–11284. (b) Riegler, H.; Spratte, K. *Thin Solid Films* **1992**, *210*, 9–12.

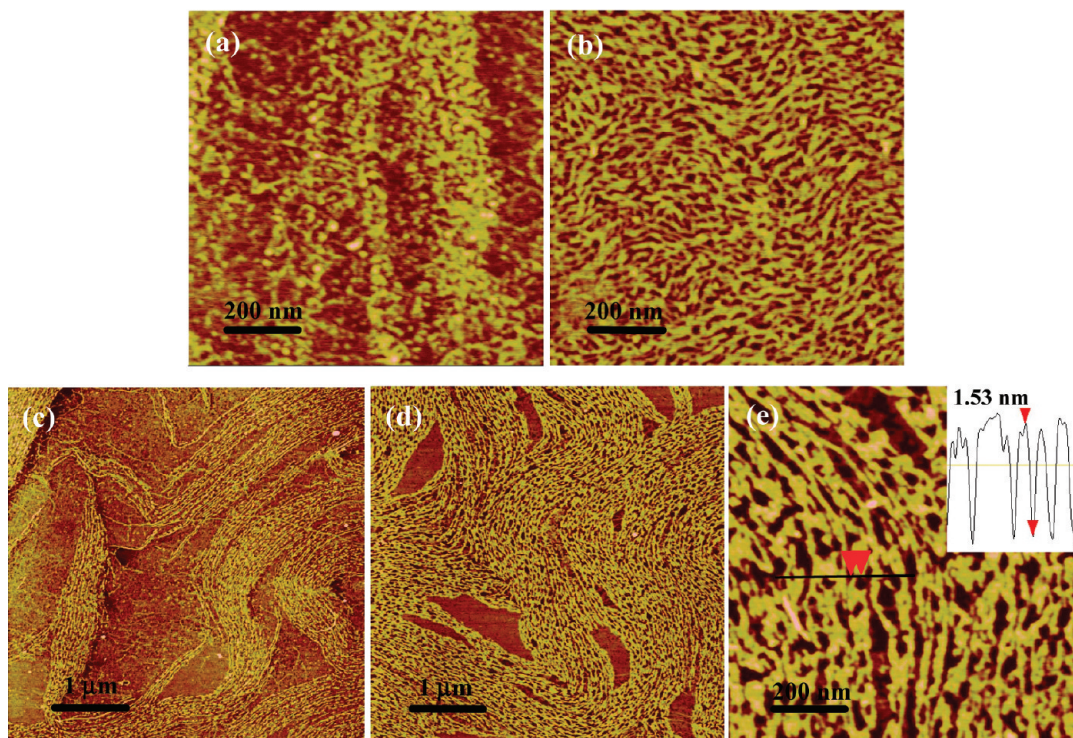


**Figure 6.** AFM images of one-layer LB films of **1b** and **1c** deposited at different surface pressure: (a) at 7 mN/m and (b) at 20 mN/m for **1b**; (c) at 5 mN/m, (d) and (e) at 10 mN/m for **1c**.

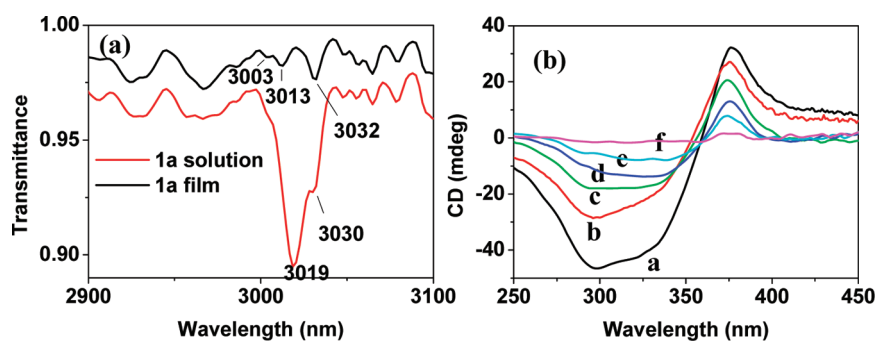


**Figure 7.** (a) FT-IR spectra of **1a** in chloroform solution and in LB films. (b) CD spectra of a 25-layer **1a** LB film deposited in pure water subphase when immersed in hydrochloric acid solution at different time intervals: (a) 0, (b) 10, (c) 30, (d) 60, (e) 100, and (f) 180 min.

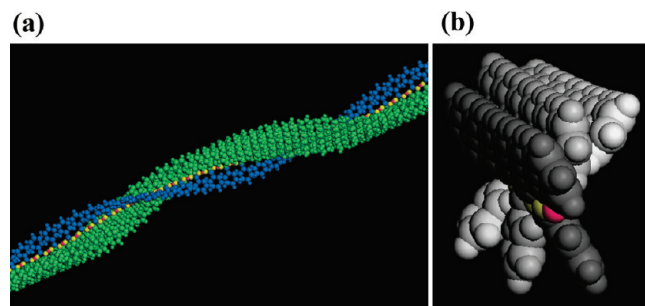


**Figure 8.** Possible model of the T-shaped rod-coil molecules for the formation of chiral LB films: (a) top view and (b) exploded front view omitted coil chains for clarity.

of the neighboring molecule. In our LB films, for example, the H-bond formation of **1a** was confirmed by the FT-IR spectra of the film. In comparison with the free N-H bond of the rod-coil molecule in the chloroform solution, which is observed at 3030, 3019  $\text{cm}^{-1}$ , the vibration band shifts obviously in the film to 3032, 3013, 3003  $\text{cm}^{-1}$  (or 3005  $\text{cm}^{-1}$  for **1c**), indicating the

H-bonding action between the rod-coil molecules (Figure 7a, Figure S6).

The chirality of LB films is stable over time. The films of **1a** prepared as described previously did not show any decrease of the CD intensity after several months, even when immersed in pure water. However, the circular anisotropy can be erased by immersing the film into hydrochloric acid (HCl) solution (Figure 7b). In HCl solution, the nitrogen in the imidazole would be protonated and the H-bonds between the molecules are destroyed. Thus, the intensity of the CD signal become weak, and finally the chirality of the film disappears as the immersing time increases. The one-layer LB film of **1a** (at 15 mN/m) on a silicon substrate was immersed in HCl solution after 3 h for protonation; AFM images show the chiral ribbons changed into irregular structures, indicating protonation disrupts the chiral assemblies (Figure S7). This further confirms that supramolecular chirality of the LB films arises from the hydrogen-bond formation between the rod-coil molecules.

An air-water interface provides a confined two-dimensional environment, which may lead to supramolecular chirality from

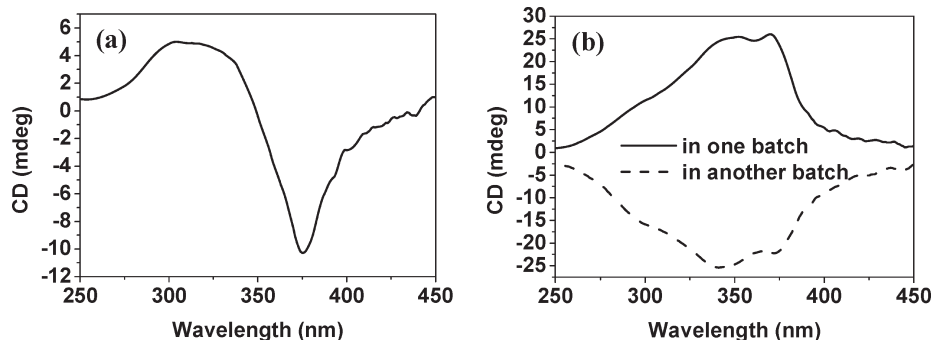


**Figure 9.** CD spectra of LB film for **1a** in different batches: (a) splitted CD signal with a positive signal at low wavelength and a negative signal at high wavelength; (b) unsplit CD signal in different batches.

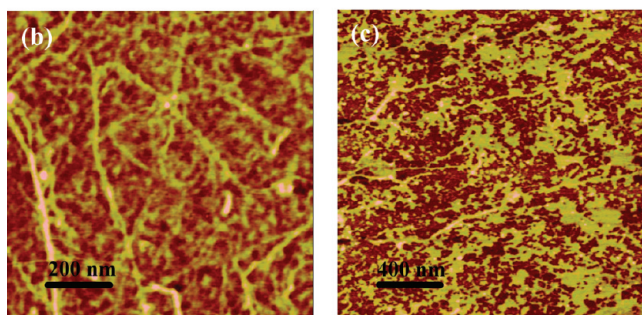
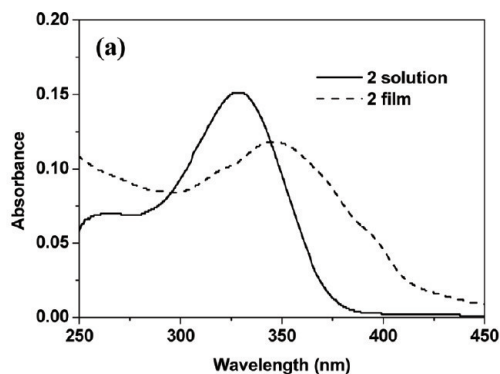


**Figure 10.** (a) UV-vis spectra of **2** in  $\text{CHCl}_3$  solution and in LB films. (b, c) AFM images of LB films of **2** deposited at surface pressure of 5 and 20  $\text{mN/m}$ , respectively.

achiral molecules.<sup>26</sup> In our case, supramolecular chirality arises most probably due to the cooperative interactions of hydrogen bond between the rod-coil molecules and  $\pi$ - $\pi$  stacking between the aromatic rod segments. The steric constraint, which arises from the large aromatic rings, weakens the intermolecular  $\pi$ - $\pi$  stacking to some extent. To relieve the steric crowdings, the neighboring aromatic segments would deviate from a certain plane. To maintain the directionality nature of the H-bond,<sup>27</sup> consequently, the adjacent rod-coil molecules tilt in the same direction as their neighbors, and then the rod-coil molecules could assemble into a helical-sense nanostructure, as shown in Figure 8. Whereas at low surface pressure, the rod segments of the molecules are flatten on the water surface and the molecules are relatively free. As a result, no CD signal was detected, and no

helix structures were observed by AFM when the films were deposited in that region.

In principle, the opportunity of molecular stacking forming the right- or left-handed helical structure is equal. However, the experimental results reveal that a chiral LB film is indeed formed. For the films fabricated in one batch, the same CD signals were observed in the different positions of the same plate. This suggests that one predominant enantiomeric assembly is formed in the whole film. If one-handedness of the aggregates is formed at the beginning, the subsequent assembly will follow that handedness due to a cooperative interaction.<sup>28</sup> However, the handedness of the starting aggregate is determined by chance.<sup>8,26,28</sup> Therefore, the opposite CD signals for the films could be fabricated in different batches (Figure 9a). Sometimes, unsplit CD signals were also observed (Figure 9b), which may suggest an irregular structure in their chiral assemblies. We have fabricated 40 batches of the LB films of **1a** and found that 19 films showed positive (47.5%) CD signals and 16 films showed negative signals (40%) around 376 nm and 5 films showed unsplit CD signals (12.5%). Such indetermination of the chirality of the films is essentially the same as those reported on the chirality of the films obtained from achiral molecules, which could be due to a spontaneous symmetry breaking.<sup>5,26,28</sup> Subsequently, due to the directionality of the H-bond, these chiral assemblies would further tilt to form supramolecular helical structures (Figure 8), thus causing macroscopic chirality.

**Comparison with 2.** To further support our conclusion, we reduced conformational rigidity of the aromatic rod segments by replacing a phenanthrene unit into a phenyl unit (**2**, Figure 1). The isotherm of the molecule also reveals a very similar behavior compared with **1a**. A shoulder appears at the surface pressure of 17  $\text{mN/m}$ , indicating the molecular reorientation. The UV-vis spectra of the 15-layer LB films deposited at 20  $\text{mN/m}$  show the red shift from 329 to 347 nm compared with that of the chloroform solution, indicating J-aggregate formation in the LB films (Figure 10a). But when the film was measured by CD spectra, no CD signal was detected. The AFM images reveal cylindrical structures at low surface pressure, and island morphologies coexisted with long cylinders at high surface pressure (Figure 10b,c). This may be due to the  $\pi$ - $\pi$  interaction and the hydrogen bond formation between the rod segments. However, the aromatic rod segments could not provide enough conformational rigidity to make the molecules deviate from a certain plane in a helical sense when the hydrogen bond is formed between the neighboring molecules. Therefore,

(26) (a) Viswanathan, R.; Zasadzinski, J. A.; Schwartz, D. K. *Nature (London)* **1994**, *368*, 440–443. (b) Yuan, J.; Liu, M. *J. Am. Chem. Soc.* **2003**, *125*, 5051–5056. (c) Zhang, L.; Lu, Q.; Liu, M. *J. Phys. Chem. B* **2003**, *107*, 2565–2569. (d) Huang, X.; Li, C.; Jiang, S.; Wang, X.; Zhang, B.; Liu, M. *J. Am. Chem. Soc.* **2004**, *126*, 1322–1323. (e) Guo, P.; Liu, M. *Langmuir* **2005**, *21*, 3410–3412.

(27) (a) MacDonald, J. C.; Whitesides, G. M. *Chem. Rev.* **1994**, *94*, 2383–2420. (b) Ajayaghosh, A.; George, S. J. *J. Am. Chem. Soc.* **2001**, *123*, 5148–5149.

(28) (a) Pawlik, A.; Kirstein, S.; De Rossi, U.; Dähne, S. *J. Phys. Chem. B* **1997**, *101*, 5646–5651. (b) von Berlepsch, H.; Böttcher, C.; Quart, A.; Burger, C.; Dähne, S.; Kirstein, S. *J. Phys. Chem. B* **2000**, *104*, 5255–5262.

no helical-sense structures are obtained, and no supramolecular chirality is detected by CD measurement.

### Conclusions

A series of achiral rod–coil molecules were synthesized, and their interfacial behaviors were investigated. For **1a** and **1b**, a shoulder appeared in the isotherms, indicating that a transformation of the aromatic rod segment of the molecule from flat-on to vertical orientation occurred upon compression. Interestingly, when the films were transferred onto solid substrates, CD spectra revealed a macroscopic chirality existed in the film deposited after the shoulder. AFM images showed ill-defined ribbons in the LB films. For **1c**, although different isotherm was obtained because the PEO chains dissolved into water upon compression, a chiral film was also achieved by deposition. In contrast, compound **2**, based on a reduced conformational rigidity of the aromatic rod segment, does not form chiral assemblies. FTIR and protonation experiments confirmed that the hydrogen bond existed in the LB films. Combining the data collected, the macroscopic chirality should be due to a cooperative interaction of hydrogen bond between the molecules and  $\pi$ – $\pi$  stacking between the

aromatic rod segments. Additionally, the steric constraints between the aromatic rod segments are crucial for chiral assembly. This research affords a better understanding of chirality at the supramolecular or macroscopic level as well as functionalization of chiral materials. Also, this work provides further insight into designing amphiphilic molecular architecture to get optical active property from optically inactive molecules at the air–water interface.

**Acknowledgment.** This work was supported by the National Creative Research Initiative Program. The BK21 program from the Ministry of Education and Human Resources Development and NSF-DMR-0646958 are gratefully acknowledged.

**Supporting Information Available:** Synthetic procedures and characterization of **1a**, **1b**, **1c**, and **2**, compression–expansion cycles of **1a**, AFM images and CD spectra of multilayers of **1a**, UV–vis spectra of **1b** and **1c**, angle dependence and FT-IR spectra of **1c**, AFM images of **1a** after immersing in HCl solution. This material is available free of charge via the Internet at <http://pubs.acs.org>.